Seismic Isolation and Protection Systems

AN EXPERIMENTAL MODEL OF BUCKLING RESTRAINED
BRACES
FOR MULTI-PERFORMANCE OPTIMUM DESIGN

Noemi Bonessio, Giuseppe Lomiento and Gianmario Benzoni
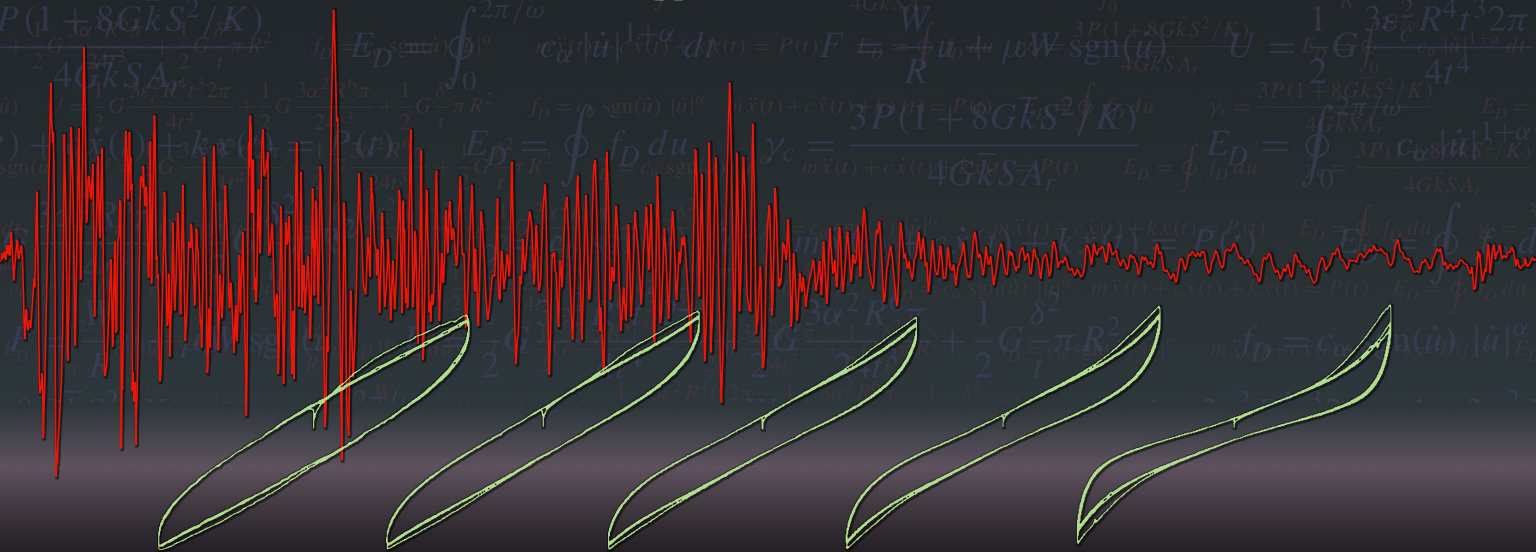
AN EXPERIMENTAL MODEL OF BUCKLING RESTRAINED BRACES FOR MULTI-PERFORMANCE OPTIMUM DESIGN

NOEMI BONESSIO, GIUSEPPE LOMIENTO AND GIANMARIO BENZONI

This paper presents the formulation of an analytical model of buckling restrained braces (BRBs) and its implementation into a structural optimization procedure in order to design the protection system of an existing structure. The procedure, based on a multi-performance approach, provides the minimum cost design solution, through sizing and topology optimization of the BRBs, for the retrofit of an existing structure. An analytical formulation for the BRBs is developed in order to introduce an efficient characterization of these devices into the structural optimization procedure. The prediction provided by the proposed analytical model is compared with the results of an experimental test campaign and the bilinear model.

1. Introduction

Passive energy dissipators such as viscous-fluid dampers, viscous-elastic dampers, metallic ductile dampers and friction dampers are widely used to reduce the dynamic response of civil engineering structures due to seismic and wind loads. The effectiveness of the dampers depends on the capability to absorb the structural vibration energy and to dissipate it through their inherent hysteresis behavior in order to reduce structural damages [Soong and Dargush 1997]. Among these dissipating devices, buckling restrained braces (BRBs) have been developed and applied for the seismic protection of building structures since their hysteretic behavior could be kept stable for cyclic tensile and compressive loads and desirable yielding forces are easily obtained by sizing their inner steel core. In addition they offer consistent energy dissipation capability and easy manufacturing, installation and maintenance [Black et al. 2002; Kiggins and Uang 2006; Lopez and Sabelli 2004; Sabelli 2001; Sabelli et al. 2003; Wada et al. 1998]. The optimal mechanical characteristics of the dampers depend on the structural configuration in which they are located, on the performance level and on the entity of the applied horizontal loads. Sizing and topology optimization procedures can be efficiently used in order to determine their characteristics and their location in a generic structural scheme.

   Recently, performance-based design is getting more importance, overcoming traditional prescriptive design methods towards full reliability-based design methodologies. The present paper uses performance-based design concepts and casts them into a multiple-objective optimization procedure. In many studies, mono- or multi-optimization tools have been applied to the structural design [Frangopol 1995; Breitung et al. 1998; Thoft-Christensen and Sorensen 1987; Fu and Frangopol 1990]. In particular, the structural optimization procedure developed in [Bonessio 2010] has been here specialized into a specific procedure to retrofit an existing structure with a BRB system. The procedure provides the minimum cost design

solution through the optimization of the braces characteristics and locations on the structure, while respecting several performance requirements. The proposed approach is based on a complete mechanical representation of the existing frame and the braces [Lomiento et al. 2010].

In many studies, the simple bilinear representation of the cyclic behavior of BRBs has shown to underestimate their actual capacity in the small deformation range [Tremblay et al. 2004; Fahnestock et al. 2004]. More accurate models, generally used to perform nonlinear time history analyses, prevent a closed-form definition of parameters commonly used in optimization procedures, such as effective stiffness and damping. For the BRBs, an original mechanical model based on experimental data is here proposed and formulated in a closed form to be easily integrated into the optimization algorithm.

2. Structural optimization procedure

The general procedure is schematized in four consecutive phases as follows:
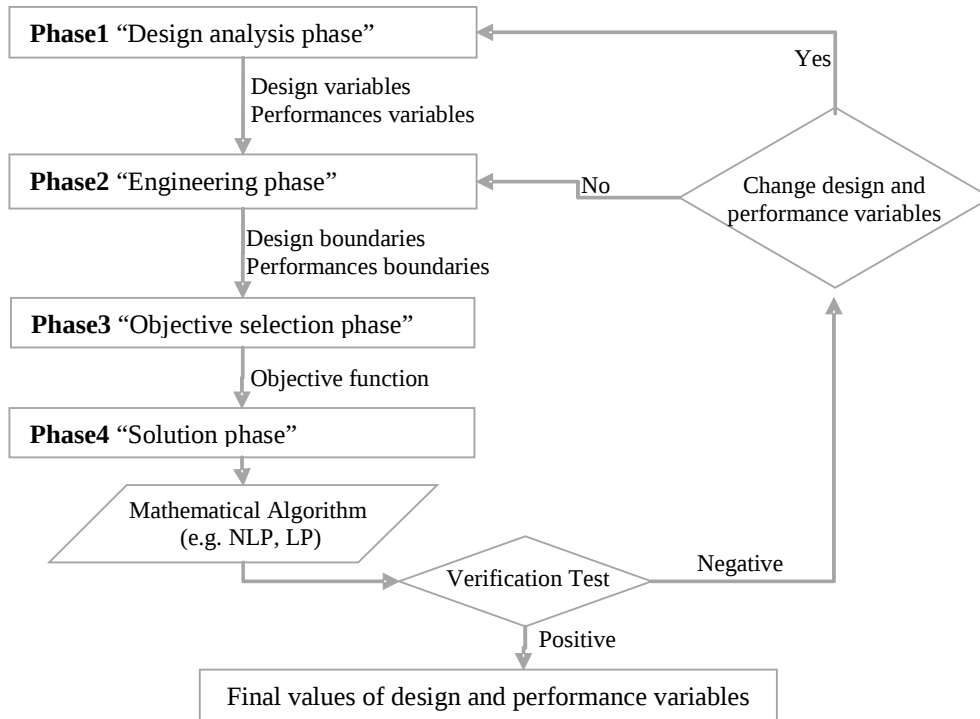
2.1. *Phase 1: Design analysis phase.* In this phase the variables involved in the optimization process are identified and defined as design variables and performance variables. The design variables are the final objectives of the optimization process while the performance variables are used to check the conformity of the structure with the performance requirements. The axial stiffness of the braces and their dissipative capacity together with their location in plan and in elevation are considered as design variables. The behavior of each dissipative brace is characterized by an effective damping ratio and an effective stiffness that will be optimized by the proposed algorithm.

The generic structural scheme consists in a three-dimensional structure with p floors ($k = 1 \ldots p$) and m columns ($j = 1 \ldots m$) for a total of $n = p(m-1)$ structural bays, available to allocate the braces; the i-th brace ($i = 1 \ldots n$) is located in the i-th structural bay, pinned or bolted to the frame.

The design variables to be optimized are stored in two vectors. The first one is the $n \times 1$ vector $\boldsymbol{k}$:

$$\boldsymbol{k} = [k_1 \, k_2 \, \ldots \, k_i \, \ldots \, k_n]^T \tag{2-1}$$

where k_i is the normalized axial stiffness of the i-th brace, given by:

$$k_i = \frac{K_i}{K_i^{\text{ref}}} \tag{2-2}$$

K_i is the axial stiffness of the i-th brace and K_i^{ref} is the axial stiffness associated with a conventional cross-sectional area used as a reference to initialize the procedure. The second $n \times 1$ vector $\boldsymbol{\xi}$ is defined as

$$\boldsymbol{\xi} = [\xi_1 \, \xi_2 \, \ldots \, \xi_i \, \ldots \, \xi_n]^T \tag{2-3}$$

where ξ_i is the damping ratio of the i-th brace. The total stiffness matrix $\boldsymbol{K}_{\text{tot}}(\boldsymbol{k}, \boldsymbol{\xi})$, condensed on the lateral displacement, and the total damping ratio of the structure $\xi_{\text{tot}}(\boldsymbol{k}, \boldsymbol{\xi})$ are considered as performance variables. The performance variables need to be express as a function of the design vectors $\boldsymbol{k}$ and $\boldsymbol{\xi}$ in order to be implemented in the optimization algorithm. These correlations are proposed by Bonessio, where parametric analyses on the global stiffness matrix and on the total damping have been performed [Bonessio 2010].

2.2. *Phase 2: The engineering phase.*

Several engineering boundaries on design and performance variables are set in the form of inequalities and equations. The design boundaries are expressed as

$$\boldsymbol{k} = [k_1 \, k_2 \, \ldots \, k_i \, \ldots \, k_n]^T \geq \boldsymbol{0}, \tag{2-4}$$

$$\boldsymbol{\xi} = [\xi_1 \, \xi_2 \, \ldots \, \xi_i \, \ldots \, \xi_n]^T \geq \boldsymbol{0}, \tag{2-5}$$

$$\xi_i = f_i(k_i) \quad \text{for} \quad i = 1 \ldots n. \tag{2-6}$$

Equations (2-4) and (2-5) express a physical limitation on stiffness and damping ratio, valid for all type of braces. The set of equations (2-6) is specific for the particular type of braces used and represents the correlation between effective stiffness and damping ratio, as formulated in the next paragraph for the BRBs. The accuracy of the mechanical model of the braces influences the optimum values of the design variables and consequently the efficiency of the earthquake protection system. The performance boundaries are inequalities that involve the performance variables $\boldsymbol{K}_{\text{tot}}(\boldsymbol{k}, \boldsymbol{\xi})$ and $\xi_{\text{tot}}(\boldsymbol{k}, \boldsymbol{\xi})$:

$$\bar{\boldsymbol{p}} \leq \boldsymbol{K}_{\text{tot}}(\boldsymbol{k}, \boldsymbol{\xi}) \cdot \bar{\boldsymbol{u}}, \tag{2-7}$$

$$\xi_{\text{tot}}(\boldsymbol{k}, \boldsymbol{\xi}) \leq \bar{\xi}_{\text{tot}} \tag{2-8}$$

where $\bar{\boldsymbol{p}}$ is a vector of assigned lateral loads, for each performance level, $\bar{\boldsymbol{u}}$ is the vector of the maximum allowable displacements, and $\bar{\xi}_{\text{tot}}$ is the maximum allowed damping ratio.

2.3. *Phase 3: The objective selection phase.* The definition of the objective of the design procedure represents the goal of this phase. For this application the objective is the cost-minimization of the protection system. The cost W of the system is mainly associated with the size of the braces and consequently related to their stiffness:

$$W(\boldsymbol{k}) = \boldsymbol{c}^T \boldsymbol{k} \tag{2-9}$$

where the vector $\boldsymbol{c}^T = [c_1 \, c_2 \, \ldots \, c_i \, \ldots \, c_n]$ includes information about the geometry and the material properties of the braces.

2.4. *Phase 4: The solution phase.* The final phase consists of the evaluation of the optimal numerical values for the design variables. For instance, for the sizing and topology optimization of a BRB protection system, a standard nonlinear programming (NLP) problem has to be solved. The sequential solution technique is proposed as a tool to treat the NLP problem as a linear programming problem [Bonessio 2010]. The generic formulation of the problem, in agreement with the classical format of mathematical programming, is expressed as follows, using equations (2-1) to (2-9):

$$\begin{aligned}
&\text{Find } k_1, k_2, \ldots k_n \text{ and } \xi_1, \xi_2, \ldots \xi_n \\
&\text{minimizing } W(\boldsymbol{k}) = \boldsymbol{c}^T \boldsymbol{k} \\
&\text{subject to } \boldsymbol{k} \geq \boldsymbol{0}, \\
&\qquad\qquad \boldsymbol{\xi} \geq \boldsymbol{0}, \\
&\qquad\qquad \bar{\boldsymbol{p}} \leq \boldsymbol{K}_{\text{tot}}(\boldsymbol{k}, \boldsymbol{\xi}) \cdot \bar{\boldsymbol{u}}, \\
&\qquad\qquad \xi_1 = f_1(k_1), \; \ldots, \; \xi_n = f_n(k_n).
\end{aligned} \tag{2-10}$$

The procedure is able to determine the stiffness k_i and the damping ratio ξ_i of the brace placed in the i-th location of the frame, for a maximum of n braces in the n possible locations. In the allowable set of values for each design variable k_i, zero values is also included. This allows some of the n braces to be eliminated so topology of the protection system can also be optimized.

3. Experimental characterization

3.1. *Specimens and testing protocol.* A total of 3 sets A, B and C of full-scale specimens were tested, each set comprising two nominally identical specimens. Each specimen was composed of a central core plate, which was confined in a concrete-filled square hollow square section with different characteristics in terms the yield strength of core F_{ya}, the cross sectional area A and the lengths L_{b}, L_{c}, L_{e}, L_{t}, L_{y} referred to different portions of the brace, as shown schematically in Figure 1.

The devices were tested at the Caltrans SRMD Testing Facility, at the University of California San Diego campus, that consists of a 6 DOFs shaking table specifically designed for full scale testing of isolators and energy dissipators. The displacement range of the table in longitudinal direction is ± 1.22 m with a maximum horizontal capacity of 9,000 kN. The peak velocity of the table longitudinal motion is 1.8 m/s. The installation procedure of the devices on the testing machine is consistent with the standard installation of BRBs. The ends of each brace were spliced to a cruciform gusset bracket by high-strength bolts. Both the gusset plates on the specimen and on the connection were sandblasted to a Class B faying surface [AISC 1998]. Figure 2 shows the testing rig configuration. More information about the testing rig is provided in [Benzoni and Seible 1998].
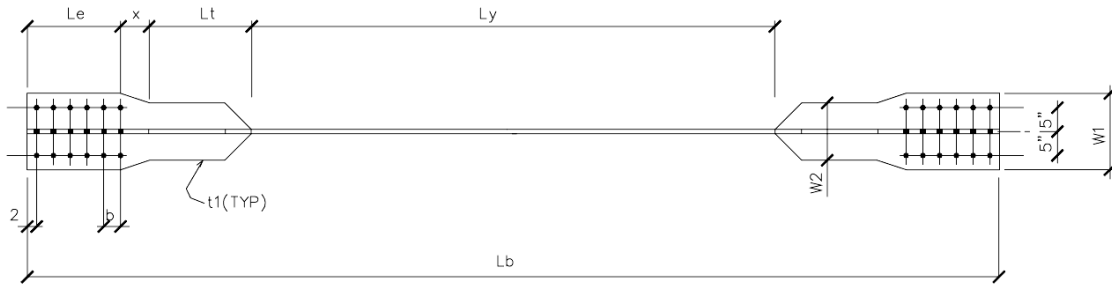
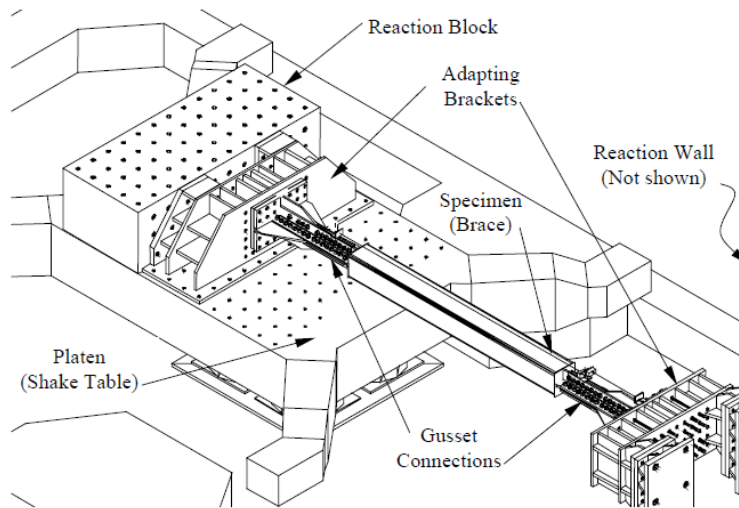**Figure 1.** Layout of the central core plate of the test specimens.

Figure 2. SRMD testing rig configuration.

A matrix of performed tests is presented in Table 1. The loading sequence was chosen accordingly to the *Recommended Provisions for Buckling-Restrained Braces* [SEAOC-AISC 2001].

Displacement level	D1	D2	D3	D4	D5	D6
Number of cycles	6	4	4	4	2	2
Brace specimen A1	12.7	20.3	38.1	50.8	77.7	88.1
A2	12.7	20.3	38.1	50.8	77.7	88.1
A3	12.7	20.3	38.1	50.8	81.3	95.3
A4	12.7	20.3	38.1	50.8	81.3	95.3
A5	12.7	20.3	38.1	50.8	81.3	88.1
A6	12.7	20.3	38.1	50.8	81.3	88.1

Table 1. Shake table peak input displacements (mm).

3.2. *Experimental and theoretical results.* Experimental results in terms of effective stiffness and damping ratio are reported in Figures 3 and 4. Each parameter is presented as a function of the ductility level μ_Δ and compared with a theoretical value obtained from a bilinear model. The force-deformation relationship of BRBs is generally presented in literature as a bilinear relationship characterized by three terms: an elastic stiffness K_1, a plastic stiffness $K_2 = \alpha K_1$, where α is the post-yielding ratio, and a yielding displacement

$$d_y = \frac{F_y}{K_1},$$

where F_y is the yielding force [Black et al. 2002; Kiggins and Uang 2006; Sabelli et al. 2003]. Using the bilinear model the relationship between the effective secant stiffness and the damping ratio with ductility can be written in a closed form. Accordingly, the theoretical value of the effective stiffness K_{eff} is obtained as a function of the displacement ductility μ_Δ:

$$K_{\mathrm{eff}} = \begin{cases} K_1 & \text{for } 0 \leq \mu_\Delta < 1, \\ K_1 \dfrac{1+\alpha\,(\mu_\Delta - 1)}{\mu_\Delta} & \text{for } \mu_\Delta \geq 1, \end{cases} \qquad (3\text{-}1)$$

with $\mu_\Delta = d_{\max}/d_y$, where $d_{\max}$ is the maximum displacement experienced during a deformation cycle. Similarly the damping ratio is given by

$$\xi_{\mathrm{eff}} = \begin{cases} 0 & \text{for } 0 \leq \mu_\Delta < 1, \\ \dfrac{2}{\pi} \dfrac{(1-\alpha)\,(\mu_\Delta - 1)}{[1+\alpha\,(\mu_\Delta - 1)]\,\mu_\Delta} & \text{for } \mu_\Delta \geq 1. \end{cases} \qquad (3\text{-}2)$$

In Figure 3, K_{eff} normalized to the elastic stiffness K_1 is reported versus the ductility term μ_Δ. The trend line, obtained as least-squares fit of the experimental data, is lower than the theoretical prediction (solid line) for ductility levels lower than 6. The peak variation in the ductility range between 1 and 2 is about 30%. In Figure 4, the theoretical values for ξ_{eff} under-estimates the experimental values for ductility levels lower than 2, while over-estimates test results for higher ductility.
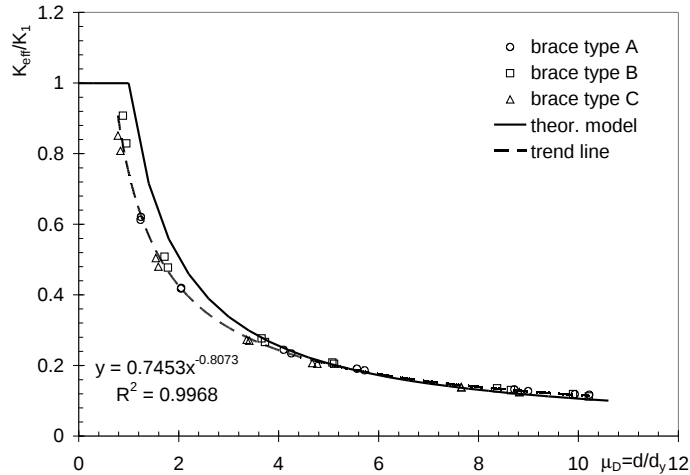

Figure 3. Normalized effective stiffness versus displacement ductility.
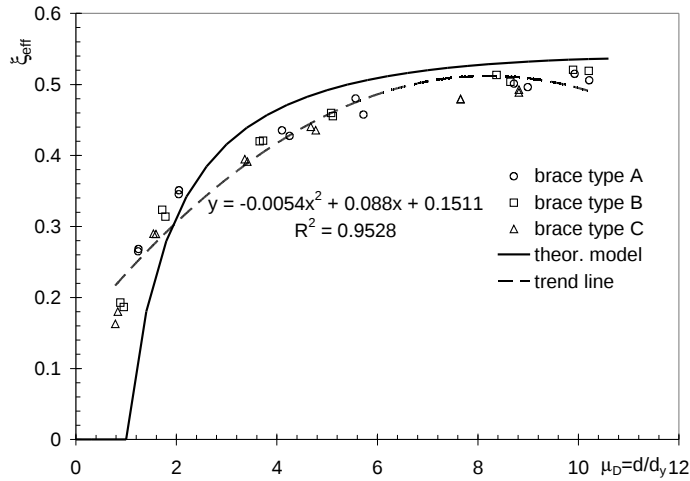
Figure 4. Damping ratio versus displacement ductility.

The relationship between the damping ratio and the effective stiffness generally indicated in equation (2-6) can be expressed as

$$\xi_{\text{eff}} = \frac{2}{\pi} \frac{(1-\alpha)\,(\mu_\Delta - 1)}{[1+\alpha\,(\mu_\Delta - 1)]^2} \frac{K_{\text{eff}}}{K_1} \tag{3-3}$$

The values of $\xi_{\text{eff}}/(K_{\text{eff}}/K_1)$ computed by this equation are compared with the experimental results in Figure 5 where the disagreement between theoretical and experimental data is clearly visible.

The theoretical ratio $\xi_{\text{eff}}/(K_{\text{eff}}/K_1)$ underestimates the experimental evidence for displacement ductility lower than 2.5 and overestimates the response for higher ductility levels.
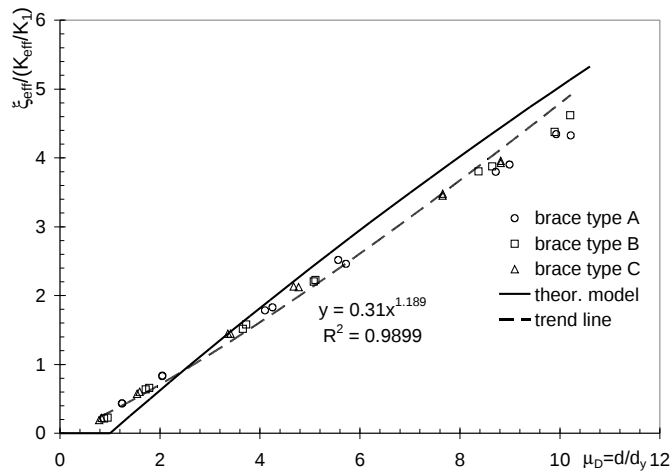
Figure 5. Ratio $\xi_{\text{eff}}/(k_{\text{eff}}/K_1)$ versus displacement ductility.

4. Discussion of experimental results and proposed model

Some of the previous observations can be organized and generalized in order to suggest an alternative analytical model of the device performance. In Figure 6 the force-displacement loops for specimen A1 are reported. The same curves are reorganized in Figure 7 after a bias with respect to the negative displacement at zero force. It can be noted the difference between the idealized and the actual response in the transition from the elastic to the plastic behavior. This difference is the main cause of the poor agreement between theoretical and experimental values for the effective stiffness and the damping ratio.

In Figure 8(a), in order to compare the effective force-displacement performance with the theoretical response, only the portion of the cycles with increasing force is plotted with a continuous line. The similarity of the curves for different specimens appears evident by using normalized forces F/F_y and
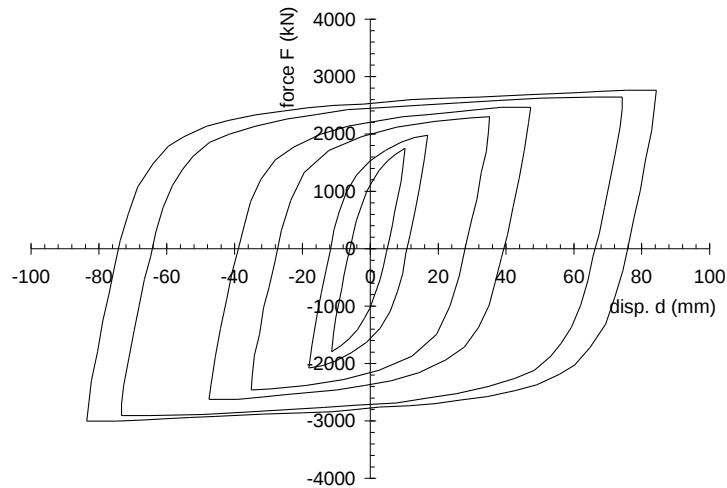
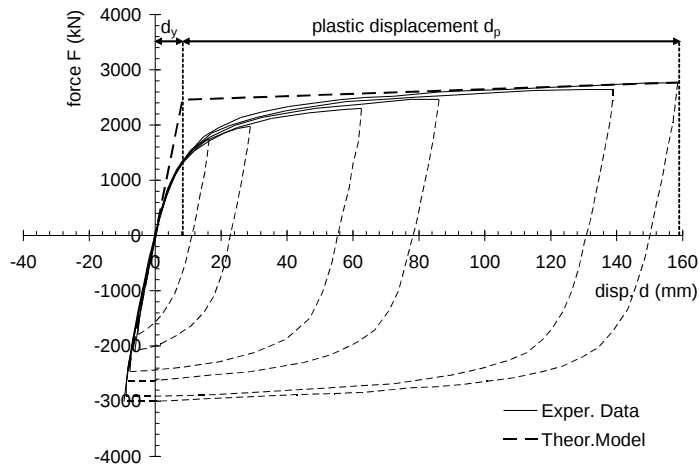**Figure 6.** Experimental data for specimen A1.

Figure 7. Experimental data and idealized response for specimen A1.

displacement ductility $\mu_\Delta = d/d_y$. The average values and the relative 95% confidence interval are reported in Figure 8(b).

The error of the bilinear model in terms of normalized forces over the whole ductility range is represented in Figure 9. As expected, the maximum errors occur at the yielding displacement. The average curve indicates a peak error approximately 45% of the yielding force. To improve the agreement between experimental and theoretical loops, a hysteretic function z was introduced. The function describes the transition from the elastic and the plastic phase and a force-displacement relationship can be proposed as

$$F = \alpha \cdot K_1 \cdot d + (1-\alpha) \cdot F_y \cdot z, \tag{4-1}$$

where K_1 is the elastic stiffness, F_y is the yield force, α is the ratio of post-yield stiffness to elastic
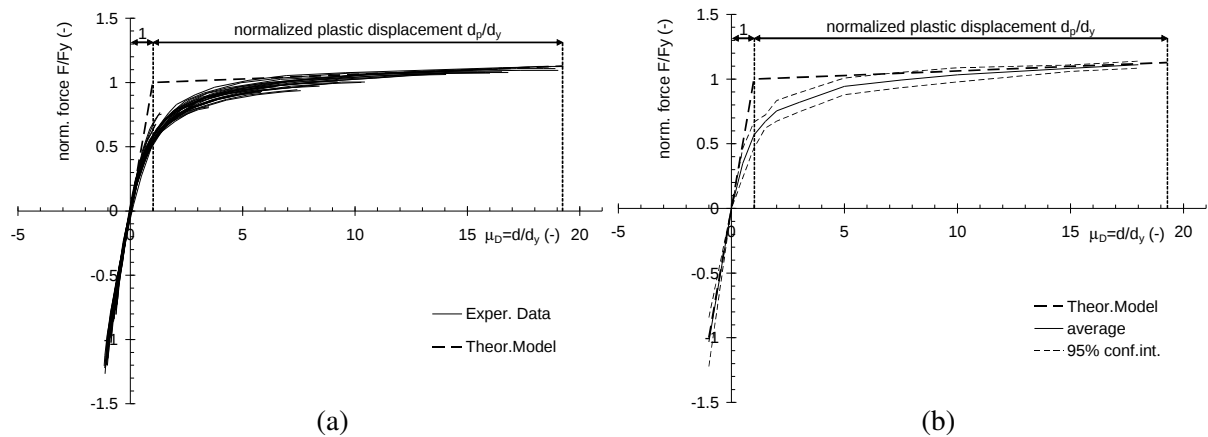

Figure 8. Normalized force-displacement curves: (a) curves for all the specimens and (b) average values and 95% confidence interval.
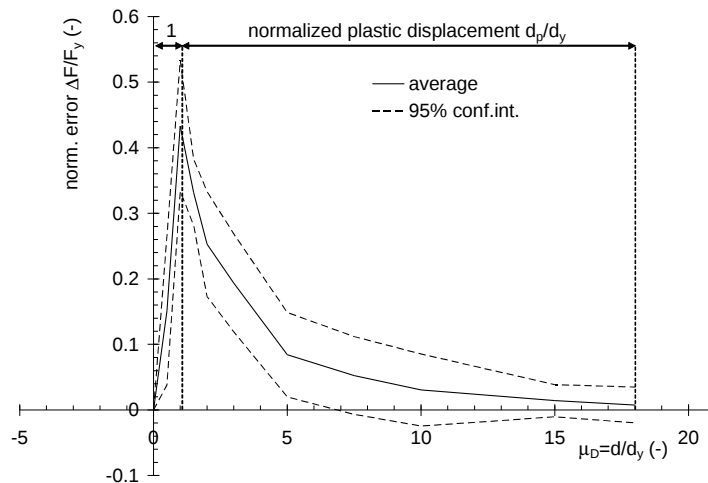

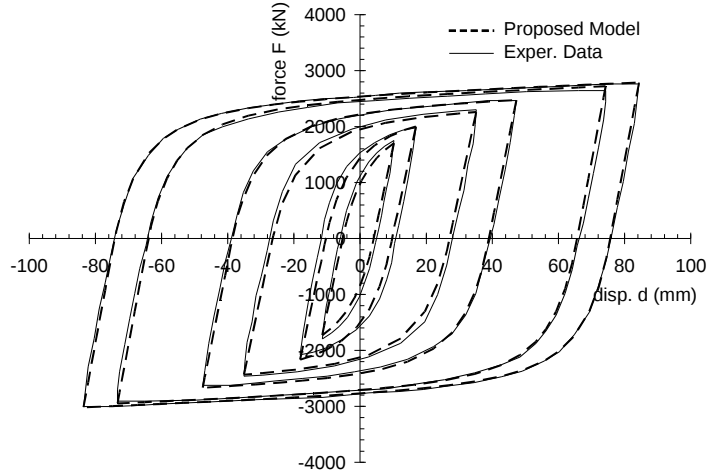**Figure 9.** Normalized errors of the bilinear model.

Figure 10. Comparison between theoretical and experimental loops.

stiffness and z is the hysteretic internal strain-dependent function, ranging from -1 and 1, with the yield surface represented by $|z| = 1$.

The function z is defined as

$$z = \frac{1}{2} \cdot \left(\frac{\dot{d}}{|\dot{d}|} - \frac{d}{|d|} \right) + \frac{1}{2} \cdot \left(\frac{\dot{d}}{|\dot{d}|} + \frac{d}{|d|} \right) \cdot \left[1 - \left(\frac{\beta + \bar{d}/d_y}{\beta} \right)^{-\beta} \right], \qquad (4\text{-}2)$$

where $\bar{d}$ is the displacement measured from the last change in the velocity sign and the parameter $\beta > 1$ is obtained experimentally and controls the shape of the transition curve from the elastic to the plastic phase. For the specific results of this study, the value $\beta = 2$ was used.

In Figure 10 the predicted force-displacement loops are presented with a dashed line in comparison with the experimental curves for the brace type A1.

According with the proposed model, the relationship between the normalized effective stiffness and the damping ratio with the displacement ductility μ_Δ can be written as

$$K_{\text{eff}} = K_1 \frac{\gamma + \alpha \, (\mu_\Delta - \gamma)}{\mu_\Delta}, \qquad (4\text{-}3)$$

$$\xi_{\text{eff}} = \frac{2}{\pi} \frac{(1 - \alpha) \, (\mu_\Delta - \delta)}{[\gamma + \alpha \, (\mu_\Delta - \gamma)] \, \mu_\Delta}, \qquad (4\text{-}4)$$

where

$$\gamma = 1 - \left(\frac{\beta + 2\mu_\Delta - x}{\beta} \right)^{-\beta} < 1, \qquad (4\text{-}5)$$

$$x = 1 - \left(1 + \frac{\mu_\Delta}{\beta} \right)^{-\beta} < 1, \qquad (4\text{-}6)$$

$$\delta = \frac{1}{2} \left[x + \frac{\beta}{1 - \beta} \left(\frac{\beta + 2\mu_\Delta - x}{\beta} \right)^{-\beta} - \frac{\beta}{1 - \beta} + \frac{x^2}{2} \right]. \qquad (4\text{-}7)$$
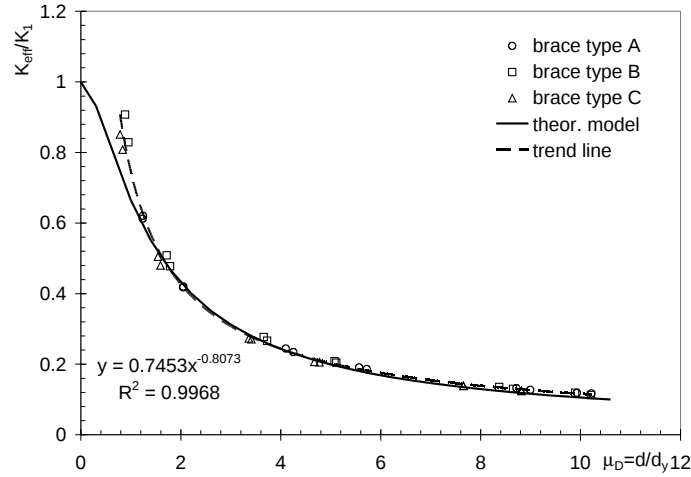
Figure 11. Normalized effective stiffness versus displacement ductility from experimental data and proposed model.
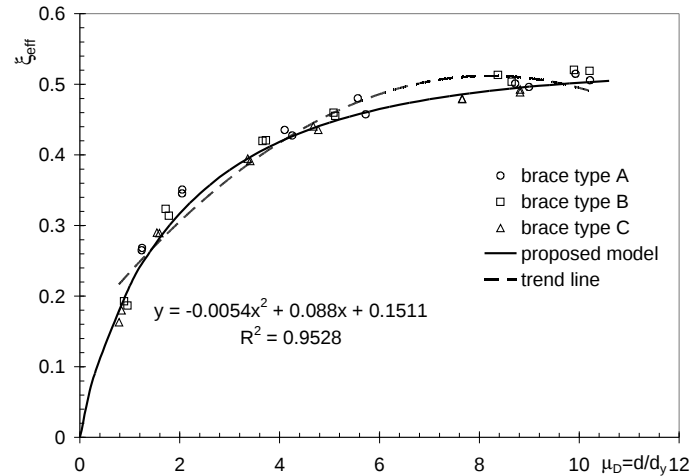

Figure 12. Damping ratio versus displacement ductility from experimental data and proposed model.

Equations (4-3) and (4-4) for the effective stiffness and damping ratio appear similar to equations (3-1) and (3-2), for the bilinear model, but take in account the smooth transition between the elastic and the plastic phase by means of the parameters γ and δ. The normalized stiffness and damping ratio predicted by using the proposed model fit well the experimental results, as shown in Figures 11 and 12, respectively.

From equations (4-3) and (4-4) the relationship between the damping ratio and the effective stiffness normalized to the elastic stiffness can be obtained as

$$\xi_{\mathrm{eff}} = \frac{2}{\pi} \frac{(1-\alpha)\,(\mu_\Delta - \delta)}{[\gamma + \alpha\,(\mu_\Delta - \gamma)]^2} \frac{K_{\mathrm{eff}}}{K_1}. \tag{4-8}$$
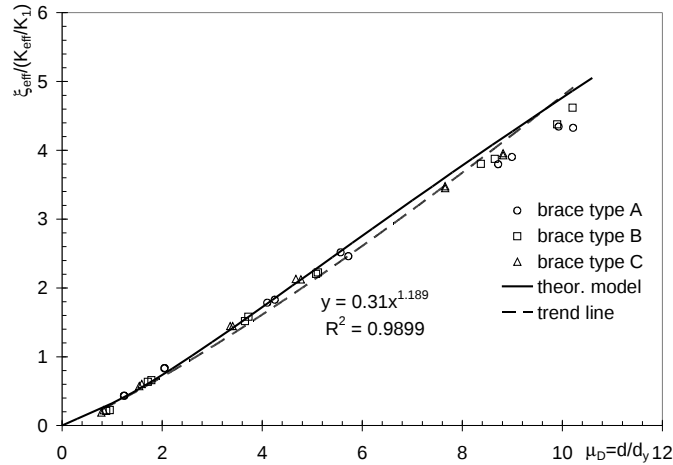
Figure 13. Ratio $\xi_{\mathrm{eff}}/(k_{\mathrm{eff}}/K_1)$ versus displacement ductility from experimental data and proposed model.

Values predicted by equation (4-8) are consistent with experimental results and are represented in Figure 13 versus the displacement ductility.

Equation (4-8) can be expressed in an implicit form for a generic i-th BRB as

$$\xi_i = f_{\mathrm{BRB}}\,(k_i) \tag{4-9}$$

where $k_1 = K_{\mathrm{eff}}/K_i$ is the normalized axial stiffness of the i-th BRB. Equation (4-9) is used in the optimization procedure for the design of the BRBs, where ξ_i and k_i are the design variables to be optimized.

5. Numerical case study for procedure validation

A simple structure is presented in order to show an application of the optimization procedure for BRBs in conformity with the multi-performance design philosophy. The structure consists of a single span-two floors frame subjected to horizontal loads. The whole system has 10 DOFs since the beam is assumed axially rigid, as indicated in Figure 14. Values of the material properties for the beam and columns
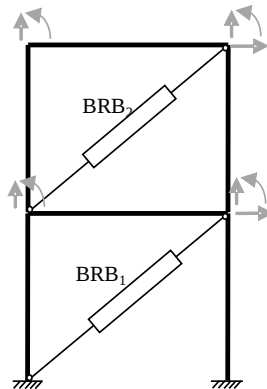

Figure 14. MDOF frame case study.

elements were selected as follows: $E = 30,000$ MPa; Poisson ratio $\nu = 0.25$. The beams have a length of 4 m and a rectangular cross-sectional area of 30×50 cm while the columns have a height of 3 m with a rectangular cross-sectional area of 30×50 cm. The optimization problem consists in the sizing of the two BRBs, 5 m long, pinned to the frames. Two allowable locations for the braces are considered, 1st floor and 2nd floor, for a total of 4 possible topology configurations for the braces (i.e., on each floor, on the 1st floor only, on the 2nd floor only, and nowhere).

The design problem has four design variables, i.e., the damping ratios ξ_1, ξ_2 and the axial stiffnesses k_1 and k_2 for the 1st and 2nd floor braces, respectively.

The optimization problem to be solved in this case study is a nonlinear programming problem expressed as

$$\text{Find } k_1, k_2, \xi_1, \xi_2$$

$$\text{minimizing } k_1 + k_2$$

$$\begin{aligned} \text{subject to } & [k_1 \ k_2] \geq \mathbf{0}, \\ & [\xi_1 \ \xi_2] \geq \mathbf{0}, \\ & \bar{\boldsymbol{p}} \leq \boldsymbol{K}_{\text{tot}}(k_1, k_2, \xi_1, \xi_2) \cdot \bar{\boldsymbol{u}}, \\ & \xi_1 = f_{\text{BRB}}(k_1), \\ & \xi_2 = f_{\text{BRB}}(k_2). \end{aligned} \qquad (5\text{-}1)$$

The vectors $\bar{\boldsymbol{p}}$ and $\bar{\boldsymbol{u}}$ represent the assigned seismic actions and the limit displacements defined for each performance level. Four levels, named Operational (O), Immediate Occupancy (IO), Life Safety (LS) and Collapse Prevention (CP), are considered [ASCE/SEI 2007]. The corresponding four levels of seismic actions are associated with the probability of exceedance of 50%, 20%, 10% and 2% in 50 years, respectively. Elastic spectra on soil type A from Eurocode 8 [CEN 2004] were used to represent seismic actions. The four sets of limit displacements are consistent with the limit drifts of 0.2%, 0.5%, 1.5% and 2.5%.

The correlation between damping ratio and axial stiffness for each BRB is established through the function f_{BRB} as indicated in (4-9) by assuming the values of α and β equal to 0.007 and 2, respectively.

The sequential solution technique and then the simplex method is applied to determinate the optimal values of the design variables, reported in Table 2 for each performance level.

The cross-sectional areas of the BRB central cores corresponding to the identified values of stiffness and damping ratio are 2.54 cm^2 and 1.61 cm^2 for the 1st and 2nd floor respectively, being the area of the 1st floor brace 1.58 times the area of the 2nd floor brace.

In order to validate the obtained design solution, a nonlinear finite element model of the structure equipped with BRBs has been carried out. For each performance level, seven ground motions were selected by means of specialized software in order to obtain an average acceleration spectrum matching the elastic design spectrum [Gasparini and Vanmarcke 1976]. The results in terms of displacement ductility of the braces and average values of the interstorey drifts are reported in Table 3 for each performance level.

From the results, it should be noted that the BRBs exceed the yielding displacement ($\mu_\Delta \geq 1$) only in the Life Safety and Collapse Prevention performance levels. The maximum displacement ductility

Performance level	Normalized stiffness k_i		Damping ratio ξ_i	
	1st floor	2nd floor	1st floor	2nd floor
FO	2.46	1.56	5.0%	4.8%
O	2.16	1.38	12.9%	12.6%
LS	1.28	0.80	28.3%	27.7%
CP	0.85	0.55	34.5%	33.2%

Table 2. BRB characteristics for each performance level.

Performance level	Displ. ductility $\mu_{\Delta,i}$		Interstorey drift	
	1st floor	2nd floor	1st floor	2nd floor
FO	0.22	0.22	0.20%	0.20%
O	0.54	0.54	0.50%	0.50%
LS	1.64	1.62	1.49%	1.45%
CP	2.75	2.70	2.51%	2.33%

Table 3. Displacement ductility and interstorey drifts for each performance level.

demand is 2.75, corresponding to an effective damping ratio of 34.5%. According to the experimental results, significant energy dissipation ($\xi = 12.6\%$ in Table 2) was found also for the Operational Performance level, even if the yielding displacement has not been exceeded ($\mu_\Delta = 0.54$ in Table 3). The average interstorey drift respects the imposed limits, and the drift-control performed by BRBs at the upper level is even more effective, as it is evident by the lower values of interstorey drifts found at the 2nd floor.

6. Conclusion

The performance of three different typologies of BRBs at several levels of plastic deformation was studied. Experimental results were compared with the bilinear model generally used for this kind of braces. A significant difference between the actual and the predicted values, in terms of stiffness and dissipated energy, was noticed, for the tested devices. By using the bilinear idealization for the force-displacement loops of the BRBs, the predicted stiffness reached a peak 30% higher than the experimental one. The dissipated energy appeared underestimated for ductility level lower than 2 and overestimated for higher ductility level, with a maximum disagreement of approximately 15% for a ductility level around 3.

A simplified model for the force-displacement loops has been proposed and it proved able to estimate the variation of stiffness and energy dissipated per cycle with the displacement induced in the brace. By using this model, the relationship between stiffness and damping ratio of BRB systems was written in a closed form expression, suitable for use in an optimization procedure for the design of BRB equipped structures.

The optimization procedure allows the assessment of size and position of the braces for the retrofit of an existing structure. The procedure follows a multi-performance approach, and the retrofitted structure complies with several performance requirements. The design procedure and the proposed model were

applied to a simple two-stories building and led to BRBs with a cross-sectional area 58% greater at the first floor than at the second. The maximum ductility demand obtained was 2.75 at the first floor. In the case study, the average interstorey drifts computed by a finite element analysis respected the imposed limit values. The procedure appears feasible for the application on more complex structures.

References

[AISC 1998] "Manual of steel construction: load and resistance factor design", American Institute of Steel Construction, Chicago, 1998.

[ASCE/SEI 2007] "Seismic rehabilitation of existing buildings", SEI 41-06, American Society of Civil Engineers, Reston, VA, 2007.

[Benzoni and Seible 1998] G. Benzoni and F. Seible, "Design of the Caltrans Seismic Response Modification Device (SRMD) test facility", in *Proceedings of the USA-Italy Workshop on Protective Systems*, 1998.

[Black et al. 2002] C. Black, N. Makris, and I. Aiken, PEER report 2002/08, University of California, Berkeley, 2002, Available at http://nisee.berkeley.edu/elibrary/Text/1276943.

[Bonessio 2010] N. Bonessio, *Structural optimization procedure for the design of earthquake protection system*, Ph.D. thesis, Department of Civil Engineering, University of Rome La Sapienza, Rome, 2010.

[Breitung et al. 1998] K. Breitung, F. Casciati, and L. Faravelli, "Reliability based stability analysis for actively controlled structures", *Eng. Struct.* **20** (1998), 211–215.

[CEN 2004] *Eurocode 8: Design of structures for earthquake resistance - Part 1: General rules, seismic actions and rules for buildings*, EN 1998-1:2004, European Committee for Standardization, Brussels, 2004, Available at http://tinyurl.com/bs-en-1998-1-2004.

[Fahnestock et al. 2004] L. A. Fahnestock, R. Sause, J. M. Ricles, and L. W. Lu, "Ductility demands on buckling-restrained braced frames under earthquake loading", *J. Earthquake Eng. Eng. Vib.* **2**:2 (2004), 255–268.

[Frangopol 1995] D. M. Frangopol, "Reliability based optimum structural design", pp. 352–387 (Chapter 16) in *Probabilistic structural mechanics handbook*, Springer, New York, 1995.

[Fu and Frangopol 1990] G. Fu and D. M. Frangopol, "Reliability-based vector optimization of structural systems", *J. Struct. Eng.* (*ASCE*) **116**:8 (1990), 2143–2161.

[Gasparini and Vanmarcke 1976] D. Gasparini and E. Vanmarcke, "Simulated earthquake motions compatible with prescribed response spectra", technical report 76-4, Massachusetts Institute of Technology, Department of Civil Engineering, Cambridge, MA, 1976.

[Kiggins and Uang 2006] S. Kiggins and C. Uang, "Reducing residual drift of buckling-restrained braced frames as a dual system", *Eng. Struct.* **28** (2006), 1525–1532.

[Lomiento et al. 2010] G. Lomiento, N. Bonessio, and F. Braga, "Design criteria for added dampers and supporting braces", *Seismic Isol. Protective Syst.* **1** (2010), 55–75.

[Lopez and Sabelli 2004] W. A. Lopez and R. Sabelli, "Seismic design of buckling restrained braced frames", *Steel TIPS* technical report, Structural Steel Education Council, 2004, Available at http://www.steeltips.org/steeltips/tip_details.php?id=76.

[Sabelli 2001] R. Sabelli, "Research on Improving the Design and Analysis of Earthquake-Resistant Steel Braced Frames", EERI/FEMA NEHRP Fellowship Report, Earthquake Engineering Research Institute, Oakland, CA, 2001.

[Sabelli et al. 2003] R. Sabelli, S. A. Mahin, and C. Chang, "Seismic demands on steel braced-frame buildings with buckling-restrained braces", *Eng. Struct.* **25** (2003), 655–666.

[SEAOC-AISC 2001] SEAOC and AISC, "Recommended provisions for buckling-restrained braced frames", draft, 2001.

[Soong and Dargush 1997] T. T. Soong and G. F. Dargush, *Passive energy dissipation systems in structural engineering*, Wiley, Chichester, UK, 1997.

[Thoft-Christensen and Sorensen 1987] P. Thoft-Christensen and J. D. Sorensen, "Optimal strategy for inspection and repair of structural systems", *Civil Eng. Systems* **4**:2 (1987), 94–100.

[Tremblay et al. 2004] R. Tremblay, L. Poncet, P. Bolduc, R. Neville, and R. D. Vall, "Testing and design of buckling restrained braces for Canadian application", in *Proceedings of the 13th World Conference on Earthquake Engineering* (Vancouver, 2004), Earthquake Engineering Conference Secretariat Canada, 2004.

[Wada et al. 1998] A. Wada, E. Saeki, T. Takeuchi, and A. Watanabe, "Development of unbonded brace", pp. 1–16 in *Nippon Steel's unbonded braces*, Nippon Steel Corporation Building Construction and Urban Development Division, Tokyo, 1998.

NOEMI BONESSIO: nbonessio@eng.ucsd.edu
Department of Structural Engineering, University of California San Diego, La Jolla, CA 92093-0085, United States

GIUSEPPE LOMIENTO: glomiento@eng.ucsd.edu
Department of Structural Engineering, University of California San Diego, La Jolla, CA 92093-0085, United States

GIANMARIO BENZONI: gbenzoni@ucsd.edu
Department of Structural Engineering, University of California San Diego, La Jolla, CA 92093-0085, United States

SEISMIC ISOLATION AND PROTECTIVE SYSTEMS

pjm.math.berkeley.edu/siaps

Seismic Isolation and Protection Systems   vol 2, no 1, 2011